ORIGINAL ARTICLE

Reconstruction of Simulated Magnetic Resonance Fingerprinting Using Accelerated Distance Metric Learning

Elmira Yazdani [1,2], Sajjad Aghabozorgi Sahaf [1,3], Hamidreza Saligheh Rad [1,2,*] ⓘD

[1] *Quantitative Magnetic Resonance Imaging and Spectroscopy Group, Research Center for Cellular and Molecular Imaging, Tehran University of Medical Sciences, Tehran, Iran*

[2] *Department of Medical Physics and Biomedical Engineering, School of Medicine, Tehran University of Medical Sciences, Tehran, Iran*

[3] *Department of Energy Engineering, Sharif University of Technology, Tehran, Iran*

*Corresponding Author: Hamidreza Saligheh Rad
 Email: h-salighehrad@tums.ac.ir

Abstract

Purpose: Magnetic Resonance Fingerprinting (MRF) is a novel framework that uses a random acquisition to acquire a unique tissue response, or fingerprint. Through a pattern-matching algorithm, every voxel-vise fingerprint is matched with a pre-calculated dictionary of simulated fingerprints to obtain MR parameters of interest. Currently, a correlation algorithm performs the MRF matching, which is time-consuming. Moreover, MRF suffers from highly undersampled k-space data, thereby reconstructed images have aliasing artifact, propagated to the estimated quantitative maps. We propose using a distance metric learning method as a matching algorithm and a Singular Value Decomposition (SVD) to compress the dictionary, intending to promote the accuracy of MRF and expedite the matching process.

Materials and Methods: In this investigation, a distance metric learning method, called the Relevant Component Analysis (RCA) was used to match the fingerprints from the undersampled data with a compressed dictionary to create quantitative maps accurately and rapidly. An Inversion Recovery Fast Imaging with Steady-State (IR-FISP) MRF sequence was simulated based on an Extended Phase Graph (EPG) on a digital brain phantom. The performance of our work was compared with the original MRF paper.

Results: Effectiveness of our method was evaluated with statistical analysis. Compared with the correlation algorithm and full-sized dictionary, this method acquires tissue parameter maps with more accuracy and better computational speed.

Conclusion: Our numerical results show that learning a distance metric of the undersampled training data accompanied by a compressed dictionary improves the accuracy of the MRF matching and overcomes the computation complexity.

Keywords: Magnetic Resonance; Fingerprinting; Distance Metric Learning; Singular Value Decomposition.

1. Introduction

Magnetic Resonance Imaging (MRI) is an invaluable diagnostic tool that inherently creates qualitative images. To provide additional physiological data, quantitative MRI is needed. The quantitative MRI has numerous applications that provide different aspects of the tissue properties. However, quantitative MR imaging faces fundamental challenges, when long scan time is still its major problem. Therefore, it would be intended to use an alternative method that improves the quality of parameter mapping in a limited time.

Magnetic Resonance Fingerprinting (MRF) [1] is a promising paradigm that paves the way toward quantitative MR imaging. MRF applies a series of time-varying parameters in a sequence of pseudo-random pulses to create quite a few images in a single scan. With the aim of speeding the acquisition, Variable Density Spiral (VDS) [2] sampling was used to sample just a proportion of the k-space, named undersampling measurement. Therefore, the acquired images have significantly aliasing artifact.

Apart from the sequence, a predefined database called dictionary, which is a collection of simulated signal time courses was generated based on the Bloch equation or the Extended Phase Graph (EPG) formalism [3] to predict the combinations of tissue properties. Now it is time to compare every fingerprint contained in a voxel with the dictionary entries to find the best-matched entry of each voxel with the dictionary, which is done by an appropriate pattern recognition algorithm. A positive match retrieved from the dictionary is assigned as the features of the associated tissue of that voxel, which then were translated into quantitative maps such as T_1, T_2, and Proton Density (PD).

MRF suffers from undersampled data in k-space that cause aliasing artifacts in reconstructed images. The conventional MRF matching algorithm or correlation algorithm propagates these artifacts to the estimated parameter maps, which cause inaccuracy [1]. The correlation algorithm is equivalent to applying a L_2 distance. This algorithm is not always practical to find the best match between observed signals and dictionary entries. To improve the accuracy of tissue mapping Wang *et al.*[4] proposed to

use distance metric learning to learn from the undersampled training data based on an Inversion Recovery Balanced Steady-State Free Precession (IR-bSSFP) pulse sequence [1]. They proposed a Compress-Sensing (CS) framework for denoising the aliased images. Moreover, they adopted the Relevant Component Analysis (RCA) metric [5] as a superior distance metric learning compared to other metric methods such as the Discriminative Component Analysis (DCA) [6] and the Local Fisher Discriminant Analysis (LFDA) [7]. As a result, they have obtained more accurate tissue parameters compared to the correlation algorithm [1]. However, their approach is not practical in the MR clinic, since they have simulated a comprehensive dictionary of signal evolutions, so their matching faced with the problem of slowness because of an intractable database that was used to their matching framework. It is plausible that this time-consuming matching process could have influenced the results obtained.

This paper leveraged results from [8] allowing for fewer computations required for MRF reconstruction and develop an accelerated distance metric learning algorithm for dictionary matching to promote the accuracy and speed of tissue parameters estimation. We proposed to use the RCA metric algorithm for an Inversion Recovery Fast Imaging with Steady-State (IR-FISP) pulse sequence [9] with digital brain phantom measurements to improve the MRF reconstruction accuracy. Moreover, we employed the low-rank and subspace model [8] to accelerate the RCA algorithm [5] by compressing the dictionary in the time domain. In this method, the fingerprint of every voxel is matched to its nearest neighbors in the compressed dictionary with the aim of acquiring more accurate quantitative maps in a short time. We first assessed the MRF method on synthetic undersampled data. Then we compared our proposed method or the accelerated RCA algorithm with the RCA algorithm (without SVD space) and Correlation algorithm, using statistics to show which one is outperforming the other in the estimation of tissue-related parameters.

2. Materials and Methods

In the following, we, first, explain a brief overview of SVD and distance metric learning in MRF. In the

second section, we discuss our experimental setup and dictionary generation, which lead us to highly undersampled k-space measurements and a pre-calculated dictionary of all possible signal evolutions in brain tissues. We, next, discuss the dictionary matching with reviewing the matching correlation algorithm and proposing our algorithm in this domain. Finally, we use statistics to examine the performance of our simulation on a digital brain phantom. All simulation and pattern recognition codes are written in Matlab (Mathworks, Natick, MA).

2.1. Theory of SVD

The SVD of A is a real-valued factorization where U, V, and S are orthogonal diagonal matrices, respectively:

$$A_{[n \times d]} = U_{[n \times n]} S_{[n \times d]} \left(V_{[d \times d]} \right)^T$$

The closest rank-k approximation of a matrix A (under both the Fobenius norm and the spectral norm) is:

$$A_k = \sum_{i=1}^{k} \sigma_i U_i V_i^T$$

The U and V matrices are called left and right singular vectors, respectively. A_k minimizes the sum of the squares of the difference of the element A and A_k. It has been Proventhat the optimal low-rank approximation of A is [10]: $\|A_k - A\|_2 = \inf\|B - A\|_2$, where B is a $n \times d$ matrix that $rank\,(B) \le k$. Sum of the squares of singular values of A is equal to its total energy, as: $E = \sum_{i=1}^{r} \sigma_i^2$. The fraction of the preserved energy in the rank-k approximation A_k is determined by the energy ratio: $e_k = \frac{1}{E}\sum_{i=1}^{k} \sigma_i^2$.

The energy ratio retains quite a few pieces information from the described original matrix, which is useful in determining an appropriate truncation index for a low-rank approximation. By applying the SVD, the MRF dictionary will be [8]: $D = USV^T$, where U, S, and V are the same parameters as aforementioned. It is proved that the SVD space representation of the dictionary is as [8]: $D_k = DV_k$.

2.2. Theory of Distance Metric Learning

A metric or distance function defines a distance between each pair of elements of a set. A family of metrics over X is defined by computing Euclidean distances after applying a linear transformation L such that $x \rightarrow L_x$ [11]. These metrics compute squared distances as

$$\mathcal{D}_L(X^i, D^j\,) = ||L_{X^i} - L_{D^i}||_2^2$$

Which is defined as a valid metric if L is full rank and a valid pseudo-metric otherwise.

Expanding the squared distances equation:

$$\mathcal{D}_L(X^i, D^j\,) = \left\|L_{X^i} - L_{D^i}\right\|_2^2$$
$$= \left(X^i - D^j\right)^T L^T L\,(X^i - D^j)$$

This allows us to express squared distances in terms of the square matrix $\boldsymbol{M} = \boldsymbol{L}^T \boldsymbol{L}$ which is guaranteed to be positive semidefinite. In terms of M, we denoted squared distances as:

$$\mathcal{D}_M(X^i, D^j) = \left(X^i - D^j\right)^T \boldsymbol{M}\,(X^i - D^j)$$

Pseudo-metrics of this form referred to as Mahalanobis metrics [11]. By learning a Mahalanobis distance, we are able to match every observed signal with dictionary entries.

The state-of-the-art algorithms for distance metric learning include global and local methods. In this paper, we applied a global supervised distance metric learning algorithms. The supervised distance metric learning tries to learn distance metrics with pairwise constraints, or known as side information. Each constraint indicates whether two data points are relevant or irrelevant in a particular learning task. In this study, we used the RCA that learns a global linear transformation by exploiting only the relevant constraints [5]. The RCA functions take a data set and a set of positive constraints as arguments and return a linear transformation of the data space into better representation, alternatively, a Mahalanobis metric over the data space.

2.2.1. Theory of RCA

To learn an optimal distance metric between fingerprints as training samples, the RCA [6] requires fingerprints and their labels. The training fingerprints consist of fingerprints from the image sequence and their corresponding dictionary entries [6]. The observed fingerprints taken from voxel-wise images that correspond to the same dictionary are assigned the same label. In addition, the same label is given to the corresponding dictionary entries. The RCA framework [5] is described in Algorithm 1. A chunklet denotes a group of fingerprints that share the same label.

Algorithm 1. RCA

Inputs:
- **The number of training fingerprints with L different labels:** M
- **The fingerprints in the chunklet jth,:** x_{ji}
- **The number of fingerprints in the jth chunklet:** n_j
- **Desired dimensionality: n**

Outputs:
- **The transformation matrix:** A

Compute:

I. Compute the within chunklet covariance matrix

$$\widehat{C} = \frac{1}{N} \sum_{j=1}^{n} \sum_{i=1}^{n_j} (x_{ji} - m_j)(x_{ji} - m_j)^T$$

Where m_j denotes the mean of the jth chunklet.

II. Compute the optimal transformation matrix with: $\widehat{C}: W = \widehat{C}^{-\frac{1}{2}}$, **which has large weights on relevant dimensions and small weights on irrelevant dimensions.**

Return **A matrix.**

2.3. Simulation Setup

2.3.1. Bloch Response Simulation

The dynamics of the magnetization for an isochromat are described by the response of the Bloch equations by the excitation parameters. Let i = 1, …, N denote the voxels of the imaged slice. We assume that in each voxel a single isochromat dominates.

The magnetization dynamics at voxel i for an isochromat are described by the parameter set $\theta_i = \{T1_i, T2_i\} \epsilon \chi$ (tissue parameters) as living on a manifold M, where χ denotes the feasible values of T_1^i, T_2^i (relaxation times at voxel i) and $1 \leq i \leq N$.

In MRF, multiple scans are obtained from one slice of the object. We indicated the scans by a matrix $X_{[N \times T]}$, in which N is the total voxels' numbers and T is the number of frames. Let $i = 1, …, N$ denote the voxels of scanned slice. Let $X_t^i [N \times t]$ and $X_{[1 \times T]}^i$ denote the response image acquired from the voxel i, respectively at time t and for all times. Similarly, $X_t [N \times 1]$ denotes the scanned slice at time t.

The dynamics of the Bloch equations are also characterized by the excitation parameters of the pulse at time t, namely the Time of Repetition (TR), Time of Echo (TE), and Flip Angle (α) which, are known parameters and are shown in a column vector as: $\theta' = \{\alpha_j, TR_j, TE_j\}^T$, where $1 \leq j \leq T$.

The combination of both the pulse sequence characteristics and the voxel properties define the magnetization response sequence at the ith voxel when properly scaled by the proton density of voxel, $PD_i \geq 0$.

Now, signal evolutions or fingerprints of any voxel can be written as a parameter mapping from θ_i and θ' to the sequence or $X_{i,:}$ as: $X_{i,:} = PD_i B(\theta_i; \theta')_{[1 \times T]}$. Where B represents a smooth mapping induced by the Bloch equation dynamics: $B: M \rightarrow C (1 \times L)$. To be able to recover the Bloch parameters or θ_i from $X_{i,:}$, we need to define a dictionary $D_{[k \times T]}$ that consists of all possible signal evolutions, simulated by the Bloch equation. Each dictionary entry or k is normalized. Note PD of the voxel i that is not simulated in the dictionary since it is a scale for matching the observed signal from a pixel with the dictionary entries. The sequence parameters, or θ' are used for both creating the dictionary and acquiring the scanned data, or X. After pre-calculating the dictionary and acquiring fingerprints from X, it is time to match every row of X with a single row of the $D = \{D_k\}, D_k = B(\theta_i; \theta')$. A Look Up Table (LUT) is constructed that consists of tissue parameter values of the dictionary. The LUT provides an inverse for D_k such that: $\theta_i^k = LUT_B(k)$. The parameter k is the matching dictionary index. Thus, the tissue parameter maps are extracted from LUT for each $\hat{k}_i$.

2.3.2. Pulse Sequence Simulation

This experiment is based on the simulation of the data acquisition by a series of pseudo-randomized Flip Angles (FAs) and Repetition Times (TRs) to excite the spin system and acquire a series of undersampled images.

The bSSFP signal was used in the original MRF publication [1], which is sensitive to T_1 and T_2. The main problem with bSSFP is that the banding artifacts resulting from inhomogeneous fields could affect quantification. However, the FISP sequence acquires coherent steady state signals with a constant unbalanced gradient moment in each repetition time [9]. The FISP sequence does not lead to the banding artifacts that are seen in bSSFP. Without any other mechanisms to destroy the coherence of the transverse magnetization (such as RF spoiling), the sequence is sensitive to both longitudinal and transverse relaxation times. In this study, our pulse sequence structure is the IR-FISP sequence, similar to that of the original MRF–FISP [9], which is simulated using the EPG Bloch equation solver to predict the signal evolution of spins that are strongly dephased by unbalanced gradients [3]. The physical processes in the IR-FISP sequence are RF excitation, spin relaxation, and spin de-phasing. With the use of spoiler gradients, the IR-FISP sequence is robust to off-resonance effects. The acquisition length was 1000 TRs. A fixed Echo Time (TE) of 2 ms is used for all the frames. The random FAs and TRs are implemented based on the MRF-FISP paper [9], which are as follows:

A sinusoidal variation of FAs by the following pattern:

$$FA\,(n) = \sin\left(\frac{n\pi}{N_{rf}}\right) * FA_{max}$$

Where:

n: the number of flip angles from 1 to N_rf (N_rf = 200)

FA_max: the maximum flip angle that is randomly selected from 5 to 90 degrees.

The TR variation is based on a Perlin noise pattern from 11.5 to 14.5 ms. The FA and TR patterns are shown in Figure 1.
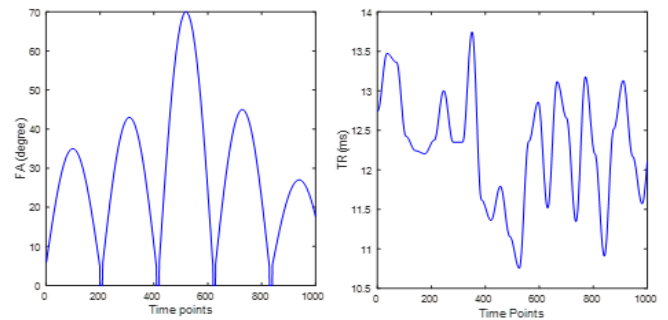
Figure 1. A sinusoidal pattern of FAs (Left side) and a Perlin noise pattern for TRs (Right side)

The chosen FA and TR patterns drive the magnetization into a persistent transient state, which is sensitive to the parameters of relaxation.

In this study, we implemented the VDS trajectory [2, 12] using minimum-time gradient design with zeroth-order gradient moment compensation [13]. We acquired under-sampled k-space data using a spiral trajectory, in which we used 24 interleaves to fully sample the inner region, and 48 interleaves to fully-sample the outer region. For every time point, each spiral trajectory is rotated by (360/48) 7.5 degrees to highly undersample the data for each time point. The undersampling ratio is 9 %, the same as the original MRF paper [1]. In order to have noisy undersampled data, we added a complex Gaussian distribution noise with zero-mean and a standard deviation of σ=0.5 to the undersampled k-space data. Therefore, the distance metric is trained with a set of images contaminated by this type of noise.

2.3.3. Digital Phantom Experiments

All experiments were performed on a digital brain phantom to investigate our method and assess the accuracy of the measurements across the acquisition, which were downloaded from the BrainWeb repository [14]. The material components of the phantoms were listed in Table 1. The phantom size is 108×90 with 90¬ slices. The 45th slice was used for training the distance metric. Slices 46 to 56 are used for validation of our method. Both the training and the testing slices are further rescaled and zero-padded to make a 128×128 image to simplify the computations. The numerical brain phantom, colored by an index is shown in Figure 2. The numerical phantom is restricted to 5 material components as listed in Table 1.
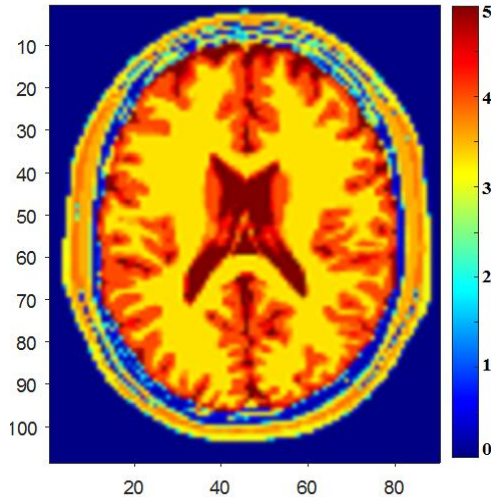
Figure 2. Slice 45 of the digital brain phantom [10] colored by index: 0 = Background, 1 = Skin/Muscle, 2 =Fat, 3 = White Matter (WM), 4 = Grey Matter (GM), 5 = Cerebrospinal Fluid (CSF) [14]

Table 1. Tissue types of digital brain phantom used from the BrainWeb website [14]

Tissue	Index	T_1 (s)	T_2 (s)	PD
Background	0	0	0	0
Muscle/Skin	1	1.1	0.035	0.7
Fat	2	Only consider water protons here		
WM	3	0.6	0.08	0.65
GM	4	0.95	0.1	0.8
CSF	5	4.5	2.2	1

Note: the T_1, T_2, and PD maps of the numerical brain phantom were known as the reference parameters in this study.

2.4. Dictionary Simulation and Generation

The FISP dictionary is simulated by the EPG formalism [3] to cover a wide range of T_1 and T_2 that contains 18,838 combinations of T_1 and T_2 of about 2 GB with the discrete parameter ranges. We outlined the T_1 and T_2 ranges and step sizes in Table 2. This range covers the total values of relaxation times that can be found in a healthy brain.

2.5. Dictionary Matching

In the experiments below we compared two different algorithms for reconstructing the image sequences. These are: (1) the original MRF algorithm or the correlation algorithm; (2) The proposed algorithm.

Table 2. The ranges and step sizes of T_1 and T_2 in the FISP dictionary

FISP Sequence	Range (ms)	Step Size (ms)
T_1	[20, 3000]	20
	[3000, 5000]	200
T_2	[10, 300]	5
	[300, 500]	50
	[500, 900]	200

Note: we computed the dictionary once, before the data acquisition, so there are no worries for time that spent in this step.

Algorithm 2. The Original MRF algorithm (Correlation algorithm)

Inputs:
- **Undersampled images:** *Y*
- **Pre-calculated dictionary:** *D*
- **Look Up Table:** LUT_B

Outputs:
- **Tissue-related parameters:** T_1, T_2, and *PD*.

Compute:

Reconstruc**t X**: $\hat{X} = F^H\{Y\}$

 for **i=1: N** *do*

 $\hat{k}_i = argmax_k\ real < D_k, \hat{X}_{i,:} > /||D_k||_2$

 $\hat{\theta}_i = LUT\ (\hat{k}_i)$

 $\hat{\rho}_t = max\left\{real < D_{\hat{k}_i}, \hat{X}_{i,:} > / \left||D_{\hat{k}_i}\right||_2^2\ , 0\right\}$

 end for

Return $\hat{\theta}, \hat{\rho}$

2.5.1. MRF Approach

The pattern-matching framework or correlation in the original MRF paper [1] is described in Algorithm 2. We generated discrete images (X) with the help of $F^H\{Y\}$, in which F{.}, H, and Y are referred to as the 2D inverse Non-Uniform Fourier Transform (NUFFT) operator [15], conjugate transpose, and undersampled images, respectively. The undersampled images of each time point are reconstructed separately using NUFFT [15].

To construct a dictionary we needed $D = \{D_k\}$, in which: $D_k = B(\theta_i^k; \alpha, TR)$ for k=1,…, P and $\theta_i^k = \{T_{1,i}^k, T_{2,i}^k, PD_i^k\}$. An LUT is constructed to provide an inverse for D_f such that: $\theta_i^k = LUT_B(k_i)$. The parameter $\hat{k}_i$, is the matching dictionary index. Thus, for each $\hat{k}_i$, the tissue parameter maps are extracted from LUT.

In this approach, the computational complexity is a major drawback of the large dictionary that leads to

inaccuracy of tissue parameters estimation. Moreover, the estimation accuracy highly depends on the accuracy of the approximate projection operator. To overcome these problems, in the next section, we offered an approach based on the accelerated distance metric learning algorithm.

2.5.5. Proposed Approach

The proposed pattern-matching framework is described in Algorithm 3. First, the dictionary or D is projected into the lower-dimensional space or the SVD space [8] by the first singular vectors or *K*. Now, the compressed dictionary is called D_k. $F^H\{.\}$ is again the 2D inverse NUFFT operator that gives us observed synthetic MR signal, or $\hat{X}_i$. Subsequently, we projected $\hat{X}_i$ to the same SVD space, resulting in K "singular images", from which we obtained compressed fingerprints, or $\hat{X}_k$. Then, the $\hat{X}_k$ is matched to the nearest neighbors in the dictionary with the help of a learned Mahalanobis distance metric A that is described in Algorithm 1. A captures fingerprint dimensions in the time domain. By measuring the dictionary index, or k_i, LUT extracted the tissue-related parameters, or $\hat{\theta}_i$ and the proton density $\hat{\rho}_i$.

2.6. Performance with Different Noises

To evaluate the noise robustness of the proposed method, we added complex Gaussian distribution zero-mean noise with different standard deviations σ = {0.3, 0.4, 0.5, 0.6, 0.7} to the undersampled k-space of all the frames.

2.7. Statistical Analysis

To assess the estimation accuracy of reconstructed parameter maps, we used following metrics:

2.7.1. Pixel-Wise Mean Absolute Relative Error (MARE) Metric

MARE metric is defined below [14]:

$$MARE = \frac{1}{n}\sum_{j}^{n}\left|\frac{A_j - P_j}{A_j}\right|$$

Where A_j and P_j denote the actual (or reference) and predicted tissue properties, respectively, at pixel jth.

Note that the reference data are the T_1, T_2, and PD maps of digital brain phantom.

Algorithm 3. Distance Metric Learning algorithm in the SVD space

Inputs:
- **Undersampled images: *Y***
- **Pre-calculated dictionary: D ($n \times t$)**
- **Matrix V_k ($t \times k$) including the first k right singular vectors of the dictionary**
- **Learned Metric: A (from algorithm 1)**

Outputs:
- **Tissue-related parameter maps: $T_1, T_2,$ and *PD*.**

Compute:

Dictionary projection to the *SVD* space:

$D_k = DV_k$

$X: \hat{X} = F^H\{Y_{:,j}\}$

Project *X* to the *SVD* space:

X: $X_k = Xv_k$

    for *i=1: N* do

    $\hat{k}_i = argmin_k||X_i/||X_i||_2^2 - D_k^k||_A$

    $\hat{\theta}_i = $ **LUT** $(\hat{k}_i)$

    $\hat{\rho}_i = \max\{real < X_i, D_{\hat{k}_i} >, 0\}$

    $X_i = \hat{\rho}_i D_{\hat{k}_i}$

    end for

Return $\hat{\theta}, \hat{\rho}.$

Note that, although we added a new step as projecting the observed signals into the SVD space in algorithm 3 compared to the algorithm 2, the amount of computation time can be significantly reduced by choosing an appropriate k.

2.7.2. Structural Similarity Index (SSIM) Metric

To measure the similarity between two quantitative maps of estimation and reference, the SSIM metric is applied [16]. The SSIM metric is based on visible structures in the image that looks at groups of pixels, since then not all of those small changes in noise and variation tend to affect groups of pixels than they do with individual pixels. The SSIM index is a decimal value between "-1" and "1", and the value of "1" is only reachable in the case of two identical sets of data (images).

3. Results

3.1. Visual Comparison

The T1, T2, and PD maps obtained by the MRF matching algorithm, and proposed MRF matching algorithms and their corresponding relative error maps

are shown in Figure 3, Figure 4, and Figure 5 respectively. The MRF matching algorithm is related to the correlation algorithm, which is used in the seminal paper [1]. In MRF-RCA, we applied the RCA algorithm [5] but it differs from the work that has been done by Wang et al. [4], since we used IR-FISP with undersampled spiral trajectory, while they used IR-bSSFP with undersampled Cartesian. The accelerated MRF-RCA is referred to as the RCA algorithm [5] that matches the fingerprints in the SVD space with a compressed dictionary in the same SVD space. To provide benchmarks for proposed algorithm, we also used fully sampled or noise free data for MRF reconstruction correlation algorithm.

3.2. The MARE Values Comparison

The MARE values of the T_1, T_2, and PD estimated by fully-sampled MRF, undersampled MRF, MRF-RCA, and accelerated MRF-RCA are shown in Table 3.

The results from Tables 3 illustrates that the proposed method has substantial gains in accuracy of reconstruction over the other [1], which better matches the reference maps. The error of fully sampled MRF results makes sense that the dictionary is quantized, while the real quantitative parameters are continuous.

According to Figure 5 and Table 3, in all algorithms, T_2 results show visible difference, which is related to CSF region. The Underestimation of T_2 value in CSF region was also reported in the original MRF experiment [1] and was justified as out-of-plane flow in this 2D experiment. A similar effect can be observed in conventional T_2 mapping techniques as well [17]. It can be seen that for T_1 and PD, the proposed algorithm (accelerated MRF-RCA) provides a better quantitative map and relative error map compared to reference map, while there is a visible difference in CSF part of T_2 relative error map.
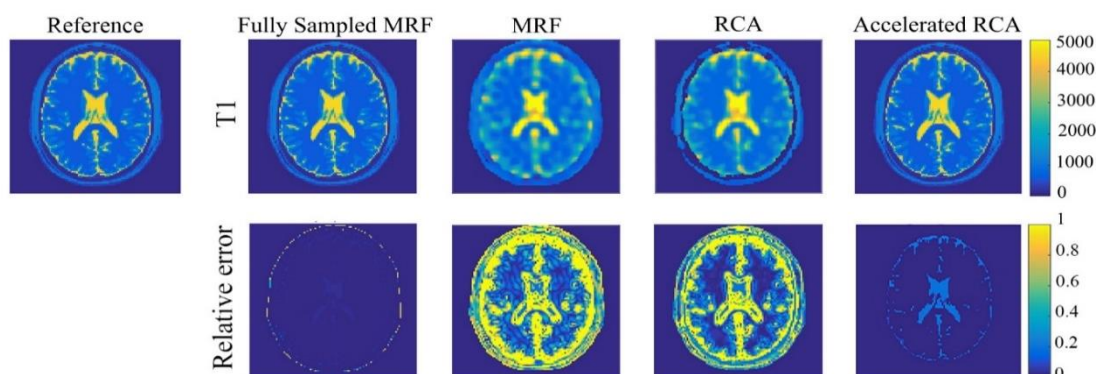
Figure 3. Reconstructed T_1 maps and corresponding relative error maps from the fully sampled MRF reconstruction, the undersampled MRF reconstruction (MRF), the MRF-RCA reconstruction, and the accelerated MRF-RCA
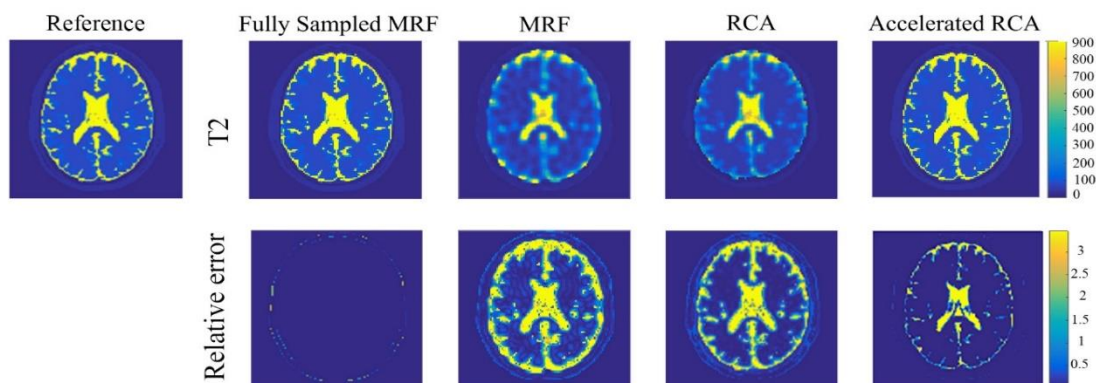
Figure 4. Reconstructed T_2 maps and corresponding relative error maps from the fully sampled MRF reconstruction, the undersampled MRF reconstruction (MRF), the MRF-RCA reconstruction, and the accelerated MRF-RCA
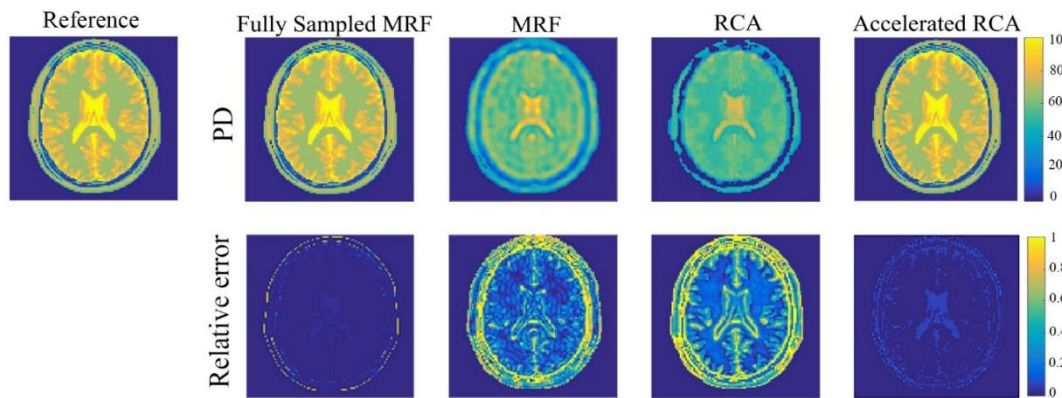
Figure 5. Reconstructed PD maps and corresponding relative error maps from the fully sampled MRF reconstruction, the undersampled MRF reconstruction (MRF), the MRF-RCA reconstruction, and the accelerated MRF-RCA

Table 3. The MARE values of T_1, T_2, and PD achieved by the MRF, MRF-RCA, and accelerated MRF-RCA

	Fully Sampled MRF	Undersampled MRF	MRF-RCA	Accelerated MRF-RCA
T_1	0.0212	0.49765	0.41554	0.05601
T_2	0.0871	0.78262	0.72071	0.10922
PD	0.0182	0.51865	0.44724	0.03406

3.3. The SSIM Values Comparison

Table 4 illustrates the SSIM values of T₁, T₂, and PD estimated by MRF, MRF-RCA, and accelerated MRF-RCA algorithms.

The results of Table 4 show that accelerated MRF-RCA has a substantial enhancement of the accuracy of tissue parameters estimation, which more desirably matches the reference maps. MRF-RCA exhibits a high level of accuracy compared to undersampled MRF. However, its performance is slower than the MRF.

3.4. Results in the Presence of Different Noises

Here we focus on the performance of proposed method in the presence of Gaussian noise on estimation of quantitative maps. The SSIM values of T₁, T₂, and PD have been illustrated in Table 5, for different standard deviations and mean of 1. Note that the results in parts 3.1-3.3 are reported in the presence of the same noise with σ=0.5. Table 5 illustrates the robustness of the proposed method in the presence of noise.

3.5. Computation Time

Computation time (Sec) of the proposed algorithm for 5 selected number of k singular values are shown in Table 6.

As expected, it is perceivable from Table 6 that the computation time increases in speed as the k value decreases. Therefore, the efficiency of the proposed algorithm in terms of speed of tissue parameters estimation is improved compared to [1]. In fact, the advantage of our proposed method is in the reduced computation time which is about 3.2 times faster than the correlation algorithm, using k=25 singular vectors. Taken together, these results show the success of our

Table 4. The SSIM values of T_1, T_2, and PD achieved by the MRF, MRF-RCA and accelerated MRF- RCA

	Fully Sampled MRF	Undersampled MRF	MRF-RCA	Accelerated MRF-RCA
T_1	0.99	0.90 ± 0.03	0.93 ± 0.04	0.98 ± 0.02
T_2	0.99	0.86 ± 0.03	0.89 ± 0.05	0.95 ± 0.02
PD	1	0.88 ± 0.04	0.90 ± 0.04	0.97 ± 0.01

algorithm at reducing the computation time while producing accurate tissue parameter maps.

Table 5. The SSIM values of T_1, T_2, and PD achieved by the proposed method in the presence of noise with 5 various standard deviations

Standard deviation	T_1	T_2	PD
0.3	0.99 ± 0.01	0.96 ± 0.02	0.98 ± 0.01
0.4	0.98 ± 0.02	0.95 ± 0.02	0.97 ± 0.01
0.5	0.98 ± 0.02	0.95 ± 0.02	0.97 ± 0.01
0.6	0.98 ± 0.03	0.95 ± 0.02	0.97 ± 0.02
0.7	0.96 ± 0.03	0.90 ± 0.03	0.95 ± 0.02

Table 6. Computation times for various values of k

K	25	50	100	150	200
Times	3.8	4.7	6.1	6.8	7.7

4. Discussion

The MRF method is a new approach to magnetic resonance and not fully exploited yet. In this work, we proposed an accelerated distance metric algorithm to reconstruct the undersampled data and estimate the MR parameters. It projects the signal evolution to the Bloch response manifold with a learned distance metric. We learned the distance metric from the data instead of a pre-defined one, which allows to better match the fingerprints to the dictionary entries. We conducted numerical simulations to demonstrate the effectiveness of our framework. We simulated an IR-FISP MRF pulse sequence with EPG formalism and implemented a distance metric learning as an MRF reconstruction algorithm, named accelerated MRF-RCA. In addition, we used the SVD based compression framework in the time domain for both the dictionary and the signal evolution compression to enable accurate MRF parameter estimates from highly undersampled data. Although works that use the low-rank structure of MRF sequences have been published in the past [8, 17-23], our technique is unique mainly in using the SVD for a distance metric reconstruction algorithm.

Our quantitative results show that in comparison to the conventional MRF matching algorithm, the distance metric learning algorithm accompanied by a compressed dictionary and signal is capable of achieving more accurate parameter map reconstruction [1, 9]. The most remarkable result to emerge from the data is that implementing an efficient technique for the dictionary compression reduces the computation time for the distance metric learning algorithm to estimate tissue parameter maps. This underlines just how important dictionary size is. Therefor the accelerated MRF-RCA outperforms MRF-RCA [4] in terms of speed. Note that the computation times reported in Table 6 were computed using the SVD approach implemented in MATLAB.

The most successful perspective of using metric learning to MRF is that some dimensions for matching may be more useful than the others. Correlations exist between each dimension of MR fingerprints and the compressed dictionary entries. Therefore, learning a distance metric can provide us important information. Furthermore, the proposed method is able to recover tissue parameter maps accurately in the presence of different noise levels. In summary, as anticipated, our results outperformed the original MRF study in term of accuracy and speed [1]. However, quantification of tissues with long T_2 such as CSF remains a challenge (due to out-of-plane flow in this 2D experiment), so another study is needed to design acquisition parameters to quantify tissues with long T_2 values.

Although our results show benefits of using a compressed dictionary during distance metric learning algorithm, the limitation of our study is that we proposed our approaches on the synthetic data; therefore, further experimental investigations are needed to estimate the tissue parameters with the proposed method.

Acknowledgements

References

1- D. Ma *et al.*, "Magnetic resonance fingerprinting," *Nature,* vol. 495, no. 7440, pp. 187-192, 2013.

2- J. H. Lee, B. A. Hargreaves, B. S. Hu, and D. G. Nishimura, "Fast 3D imaging using variable-density

spiral trajectories with applications to limb perfusion," *Magnetic Resonance in Medicine: An Official Journal of the International Society for Magnetic Resonance in Medicine,* vol. 50, no. 6, pp. 1276-1285, 2003.

3- M. Weigel, "Extended phase graphs: dephasing, RF pulses, and echoes-pure and simple," *Journal of Magnetic Resonance Imaging,* vol. 41, no. 2, pp. 266-295, 2015.

4- Z. Wang, H. Li, Q. Zhang, J. Yuan, and X. Wang, "Magnetic resonance fingerprinting with compressed sensing and distance metric learning," *Neurocomputing,* vol. 174, pp. 560-570, 2016.

5- A. Bar-Hillel, T. Hertz, N. Shental, and D. Weinshall, "Learning a mahalanobis metric from equivalence constraints," *Journal of Machine Learning Research,* vol. 6, no. Jun, pp. 937-965, 2005.

6- S. C. Hoi, W. Liu, M. R. Lyu, and W.-Y. Ma, "Learning distance metrics with contextual constraints for image retrieval," in *2006 IEEE Computer Society Conference on Computer Vision and Pattern Recognition (CVPR'06)*, 2006, vol. 2, pp. 2072-2078: IEEE.

7- M. Sugiyama, "Dimensionality reduction of multimodal labeled data by local fisher discriminant analysis," *Journal of machine learning research,* vol. 8, no. May, pp. 1027-1061, 2007.

8- D. F. McGivney *et al.*, "SVD compression for magnetic resonance fingerprinting in the time domain," *IEEE transactions on medical imaging,* vol. 33, no. 12, pp. 2311-2322, 2014.

9- Y. Jiang, D. Ma, N. Seiberlich, V. Gulani, and M. A. Griswold, "MR fingerprinting using fast imaging with steady state precession (FISP) with spiral readout," *Magnetic resonance in medicine,* vol. 74, no. 6, pp. 1621-1631, 2015.

10- G. H. Golub and C. F. Van Loan, *Matrix computations*. JHU press, 2012.

11- L. Yang and R. Jin, "Distance metric learning: A comprehensive survey," *Michigan State Universiy,* vol. 2, no. 2, p. 4, 2006.

12- H. Tan and C. H. Meyer, "Estimation of k-space trajectories in spiral MRI," *Magnetic Resonance in Medicine: An Official Journal of the International Society for Magnetic Resonance in Medicine,* vol. 61, no. 6, pp. 1396-1404, 2009.

13- B. A. Hargreaves, D. G. Nishimura, and S. M. Conolly, "Time-optimal multidimensional gradient waveform design for rapid imaging," *Magnetic Resonance in Medicine: An Official Journal of the International Society for Magnetic Resonance in Medicine,* vol. 51, no. 1, pp. 81-92, 2004.

14- C. Cocosco, V. Kollokian, R. Kwan, and A. Evans, "Brainweb: Online interface to a 3D MRI simulated brain database; http://www. bic. mni. mcgill. ca/brainweb," *NeuroImage,* vol. 5, no. 4, p. S425.

15- J. A. Fessler and B. P. Sutton, "Nonuniform fast Fourier transforms using min-max interpolation," *IEEE transactions on signal processing,* vol. 51, no. 2, pp. 560-574, 2003.

16- A. Botchkarev, "Performance metrics (error measures) in machine learning regression, forecasting and prognostics: Properties and typology," *arXiv preprint arXiv:1809.03006,* 2018.

17- C. C. Cline *et al.*, "AIR-MRF: Accelerated iterative reconstruction for magnetic resonance fingerprinting," *Magnetic resonance imaging,* vol. 41, pp. 29-40, 2017.

18- H. Zhou, L. Li, and H. Zhu, "Tensor regression with applications in neuroimaging data analysis," *Journal of the American Statistical Association,* vol. 108, no. 502, pp. 540-552, 2013.

19- B. Zhao *et al.*, "A model-based approach to accelerated magnetic resonance fingerprinting time series reconstruction," in *Proc Intl Soc Mag Reson Med*, 2016, vol. 24, p. 871.

20- C. Liao *et al.*, "Acceleration of mr fingerprinting with low rank and sparsity constraint," in *Proceedings of the 24th Annual Meeting ISMRM*, 2016, vol. 2016, p. 4227.

21- M. Doneva, T. Amthor, P. Koken, K. Sommer, and P. Börnert, "Matrix completion-based reconstruction for undersampled magnetic resonance fingerprinting data," *Magnetic resonance imaging,* vol. 41, pp. 41-52, 2017.

22- B. Zhao *et al.*, "Improved magnetic resonance fingerprinting reconstruction with low-rank and subspace modeling," *Magnetic resonance in medicine,* vol. 79, no. 2, pp. 933-942, 2018.

23- J. Assländer, M. A. Cloos, F. Knoll, D. K. Sodickson, J. Hennig, and R. Lattanzi, "Low rank alternating direction method of multipliers reconstruction for MR fingerprinting," *Magnetic resonance in medicine,* vol. 79, no. 1, pp. 83-96, 2018.